

Full Paper

Experimental and Theoretical Approaches for Interfacial Adsorption of Novel Long Chain Benzimidazolium Derivatives for Mild Steel Protection in 1 M HCl Medium

L. El Ouasif,¹ M. Laourayed,² F. Benhiba,^{3,2} M. Boudalia,² M. El Ghouli,¹ R. Achour,¹ A. Bellaouchou,² A. Guenbour,² I. Warad,⁴ and A. Zarrouk^{2,*}

¹Laboratory of Organic Heterocyclic Chemistry, (URAC 21) Pole of Competence Pharmacochimie, Faculty of Sciences, Mohammed V University in Rabat, Ibn Battuta, Avenue BP 1014 RP, Rabat, Morocco

²Laboratory of Materials, Nanotechnology and Environment, Faculty of Sciences, Mohammed V University in Rabat, P.O. Box. 1014, Rabat, Morocco

³Laboratory of Advanced Materials and Process Engineering, Faculty of Sciences, Ibn Tofail University, BP 242, 14000, Kenitra, Morocco

⁴Department of Chemistry and Earth Sciences, PO Box 2713, Qatar University, Doha, Qatar

*Corresponding Author, Tel.: +212 665 201 397

E-Mail: azarrouk@gmail.com

Received: 1 July 2020 / Received in revised form: 10 August 2020 /

Accepted: 11 August 2020 / Published online: 31 August 2021

Abstract- In this work, we are interested in the study of the anti-corrosion effect of new organic compounds of the type benzimidazolium derivatives nominated 1,3-Dinonyl-2-(nonylthio)-1H-benzimidazolium bromide (ImdC7B), 1,3-Didecyl-2-(decylthio)-1H-benzimidazolium bromide (ImdC8B) and 1,3-Didodecyl-2-(dodecylthio)-1H-benzimidazolium bromide (ImdC9B) on the corrosion of mild steel (MS) in 1 M hydrochloric acid and 1 M HCl media exploiting electrochemical techniques [polarization curves (PC) and impedance spectroscopy (IS)]. In addition to that a correlation between molecular structures and inhibitory activity was carried out exploiting the DFT (Density Functional Theory) method and molecular dynamics (MD) simulation. The results obtained show an increase in efficiency with concentration. A maximum of 94.7%, 95.7% and 96.9% is reached for a concentration of 10⁻³ M of ImdC7B, ImdC8B and ImdC9B respectively. Polarization curves studies have demonstrated that these compounds are some mixed inhibitors. The ImdC7B, ImdC8B and ImdC9B are adsorbed on the surface of MS according to Langmuir model. Reactivity parameters predicted from density functional theory calculations suggested the involvement of protonated forms of the molecules in the inhibitive process, which is also supported by the adsorption characteristics derived from MD simulations.

Keywords- Benzimidazolium derivatives; Mild steel corrosion; Electrochemical techniques; Langmuir; Theoretical study

1. INTRODUCTION

Corrosion of metals and alloys is a universally known phenomenon which causes considerable material losses, direct and indirect, each year for industry and the community. Even more serious, corrosion can cause irreversible damage to the environment and even loss of human life since it is likely to cause health problems (pollution, contamination, etc.) but also to affect devices and structures. in service (transport equipment for example) by causing serious alterations such as the general reduction in thickness, the generation of bites, but also stress corrosion cracks in welded areas or in their vicinity. All these considerations justify the interest currently shown in all fields in the fight against corrosion and also the numerous works devoted to the study of corrosion. Several organic compounds, mainly those with electronegative functional groups (containing heteroatoms) and electrons (π) with a conjugated double or triple bond, have an inhibiting effect on the corrosion of iron and steels in an acid medium. The main use of these inhibitors in acid solutions is in industrial pickling, descaling and acid cleaning processes [1-8]. Acid inhibitors require a polar group by which the molecule can adsorb and thus form a protective layer preventing corrosive agents in the aggressive environment on the metal surface, these include organic groups (O, N, S, P, amine and OH) [9-16]. The size, orientation and shape of the molecule are decisive parameters in the inhibition of corrosion [17].

A very large number of research studies have been published on transition metal complexes of benzimidazole derivatives. Some of the reports relate to their use as antifungal agents, antibacterials, antivirals etc., as well as their role in protecting metals from corrosion, several of these products have proven their ability to act as corrosion inhibitors of different metals and alloys in different aggressive media [18-21]. It is therefore from this perspective that we are interested in the study of the inhibition of corrosion by certain organic products synthesized from benzimidazole.

In this work, we are interested in the study of two new series of synthesized organic compounds such as 1,3-Dinonyl-2-(nonylthio)-1H-benzimidazolium bromide (ImdC7B), 1,3-Didecyl-2-(decylthio)-1H-benzimidazolium bromide (ImdC8B) and 1,3-Didodecyl-2-(dodecylthio)-1H-benzimidazolium bromide (ImdC9B) vis-a-vis the corrosion of MS-substrate in molar solution of hydrochloric acid. This study was carried out by coupling stationary and transient electrochemical techniques. The effect of the molecular structure of these compounds and their action on performance is compared with a theoretical calculation of the partial charges of the atoms as well as the energies of the molecular orbitals (E_{HOMO} , E_{LUMO}) and the gap energy which have been calculated. Therefore, to make the relationship between these quantum parameters and the inhibitory performance. In addition to DFT, molecular dynamics (MDS)

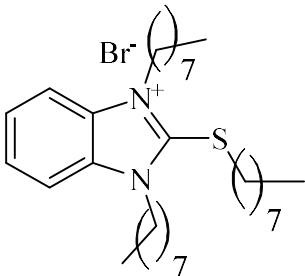
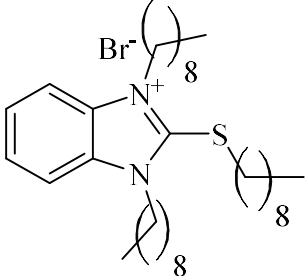
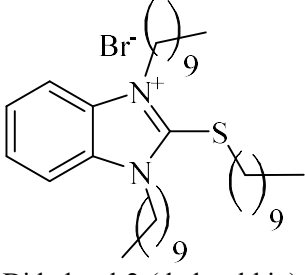
simulation allowed us to correlate molecular structure and anticorrosion activity and to estimate the mechanism of interaction between inhibitory molecules and the MS surface.

2. EXPERIMENTAL

2.1. Inhibitors Metals and aggressive solutions

Exploiting a hacksaw, we cut the metal plate (MS-substrate) to have the dimensions of 25×20×1 mm for the use of weight loss measures, and circular coupons of 100 mm² for electrochemical studies.

Table 1. Molecular structures of ImdC7B, ImdC8B and ImdC9B

Abbreviations	Structures
ImdC7B	 <p>1,3-Dinonyl-2-(nonylthio)-1H-benzimidazolium bromide</p>
ImdC8B	 <p>1,3-Didecyl-2-(decylthio)-1H-benzimidazolium bromide</p>
ImdC9B	 <p>1,3-Didodecyl-2-(dodecylthio)-1H-benzimidazolium bromide</p>

The maintenance of the metal surface before each experiment is carried out as follows, polishing, degreased, washed and dried by air. MS-substrate consist: C \cong 0.21%, Mn \cong 0.05%, P \cong 0.09%, Si \cong 0.002%, Al \cong 0.01%, S \cong 0.05% and the remaining iron.

The control corrosive electrolyte solution of 1 M HCl was prepared by appropriately diluting the stock solution of the acid (37% HCl) with distilled water. ImdC7B, ImdC8B and ImdC9B containing solutions were prepared in 1 M HCl at various concentrations of ImdC7B, ImdC8B and ImdC9B (1 μ M, 10 μ M, 100 μ M and 1000 μ M). Table 1 groups the molecular structures of the compounds studied.

2.2. Electrochemical corrosion evaluation

This experiment was carried out only at room temperature, just to have gain some insights into the electrochemical behavior of the electrode/electrolyte systems being studied. The measurements were conducted in a glass cell equipped with the working, reference and counter electrodes. The working electrode (WE) is a MS-substrate of 1 cm \times 1 cm square dimension that has been covered with epoxy resin at one side, exposing only one side with 100 mm² surface area. A $Hg, Hg_2Cl_{2(s)} / Cl^-$ (saturated KCl solution) was exploited as the reference electrode (RE), while a platinum plate was exploited as the counter electrode (CE)[22,23]. The electrochemical cell was connected to a Voltalab-PGZ 301 potentiostat/galvanostat. The open-circuit potential (OCP) of the WE in each test solution was monitored for 30 min, within which a relatively stable OCP was assumed by the electrode. The potential of the WE was polarized (potentiodynamically) between -250 mV and +250 mV, relative to the OCP at the ASTM-recommended scan rate of 0.5 mV/s.

Percentage inhibition efficiencies (%P_{PDP}) were calculated as:

$$\%P_{PDP} = \frac{i_{corr(0)} - i_{corr(i)}}{i_{corr(0)}} \times 100 \quad (1)$$

Based on the stable E_{OCP}, the electrochemical impedance spectroscopy (EIS) testing was undertaken in the frequency window of 100 kHz to 100 mHz at an AC amplitude of 10 mV. Percentage inhibition efficiencies (%P_{EIS}) were calculated as:

$$\%P_{EIS} = \frac{R_{p(i)} - R_{p(0)}}{R_{p(i)}} \times 100 \quad (2)$$

where, %P_{EIS}, and %P_{PDP} are inhibition efficiency calculated from impedance, and polarization study, respectively. Besides, $i_{corr(0)}$ are the polarization resistance, and corrosion current of blank media. Similarly, $R_{p(i)}$, $i_{corr(i)}$ are the polarization resistance, and corrosion current of inhibited medium.

2.3. DFT and MD simulation details

Numerous works have been done exploiting density functional theory (DFT) calculations to understand the effect of molecular structure on the inhibitory efficacy of organic molecules [24]. The DFT method has been exploited to correlate experimentally revealed phenomena with the characteristic of the electronic structure [25]. For this purpose, quantum chemical calculations of the desired molecule in neutral and protonated forms were done via the Gaussian 09 software package [26]. In addition, DFT calculations were performed via B3LYP and 6-311++G (d, p) basis set in the gaseous phase [27]. The quantum chemical descriptors such as E_{HOMO} , E_{LUMO} , ΔE_{gap} , global hardness (η), global electronegativity (χ), fraction of electron transferred (ΔN_{110}), and dipole moment (μ) are exploited and calculated via Benhiba et al. [28].

To estimate the interaction and adsorption proprieties of L3 molecule with the Fe (110) surface, we called upon molecular dynamics (MD) simulation exploiting the Forcite module which is included in Materials Studio (Ver.8) [29,30]. The MD simulation was executed in a 32.270* 32.270* 43.134Å³ simulation box with periodic boundary conditions, which was composed of the chemical species (with L3, 5H₃O⁺ + 5Cl⁻ + 500H₂O) and slab of Fe (110). The COMPASS force field has been exploited [31]. the system studied was performed in the presence of Andersen thermostat at 303 K, NVT ensemble, with a simulation time of 2000 ps and a time step of 1.0 fs [32].

3. RESULTS AND DISCUSSION

3.1. Polarization curves technique

Tafel curves recorded for steel electrode in 1 M HCl containing various concentrations of ImdC7B, ImdC8B and ImdC9B at 303 K are presented in Fig. 1

The polarization curves of Figure 1 show that the addition of ImdC7B, ImdC8B and ImdC9B to the corrosive medium (1 M HCl), induces a general lowering of the cathodic and anodic current densities. This effect is all the more marked when the concentration of added ImdC7B, ImdC8B and ImdC9B increases. These results suggest that ImdC7B, ImdC8B and ImdC9B reduces the anodic dissolution and delays the reduction of the H⁺ protons. In the cathodic field, the addition of inhibitors in corrosive medium results in a significant reduction in the cathodic partial current as well as a slight modification of the cathode Tafel slopes. These branches have a wide range of linearity, which proves that Tafel's law is well verified in this area. These remarks show that the reduction reaction of H⁺ protons on the surface of MS-substrate is not modified by the addition of ImdC7B, ImdC8B and ImdC9B and that it takes place according to a pure activation mechanism [33,34]. ImdC7B, ImdC8B and ImdC9B seems to adsorb first on the surface of the metal before acting by simply blocking the active sites [35,36]. In the anode domain, the addition of ImdC7B, ImdC8B and ImdC9B results in a

decrease in the anode current densities. In addition, we observe for all the studied concentrations of ImdC7B, ImdC8B and ImdC9B, the presence of two linear portions. In the first region, that of the low polarization potentials, the density of the anode current increases slightly in a limited potential domain. In the second region, that of the high potentials, once the desorption potential ($E_d \cong -0.2$ V for the three inhibitors) exceeds the anodic current density increases rapidly.

The corrosion potential (E_{cor}), the corrosion current densities (i_{cor}), the kinetic corrosion parameters (β_a , β_c resulting from the extrapolation of the anode and cathode slopes of Tafel) and the inhibitory efficacy (%PDP) are collated in Table 2.

Table 2. Polarization data of MS in 1 M HCl with / without ImdC7B, ImdC8B and ImdC9B at 303 K.

Medium	Conc. (M)	i_{corr} ($\mu\text{A cm}^{-2}$)	$-E_{corr}$ (mV/SCE)	β_a (mV/dec)	$-\beta_c$ (mV/dec)	PDP (%)
HCl	1	579.0	477.0	110	118.0	—
	10^{-3}	30.4	386.0	86.8	101.4	94.7
ImdC7B	10^{-4}	45.8	384.8	92.2	097.3	92.1
	10^{-5}	150.0	372.0	90.8	096.5	74.1
	10^{-6}	205.0	333.7	78.1	105.9	64.6
	10^{-3}	26.6	386.2	86.2	119.6	95.4
ImdC8B	10^{-4}	45.7	390.7	90.4	135.6	92.1
	10^{-5}	125.1	388.4	78.9	108.6	78.4
	10^{-6}	201.0	381.0	79.5	98.5	65.3
	10^{-3}	22.0	390.0	83.6	102.0	96.2
ImdC9B	10^{-4}	50.2	425.6	97.2	129.1	91.3
	10^{-5}	89.5	387.0	80.4	099.3	84.5
	10^{-6}	100.0	343.1	72.6	150.9	82.7

A displacement of corrosion potential (E_{corr}) is to be reported. Under these conditions, an inhibitor is generally considered to be anodic or cathodic, when the difference between the corrosion potential (E_{corr}) without and with inhibitor is greater than 85 mV [37]. In the present study, the (Table 2) reveals a displacement in the corrosion potential which exceeds 85 mV for the different concentrations of the three compounds. In addition, the values of the corrosion potential (E_{corr}) shifted towards the positive direction, thus indicate that the inhibitors in question ImdC7B, ImdC8B and ImdC9B act as inhibitors having predominantly anodic. The efficacy values increase with the concentrations of ImdC7B, ImdC8B and ImdC9B, the product ImdC9B proves to be the best inhibitor in this group with an efficacy which reaches 96.2% at 10^{-3} M.

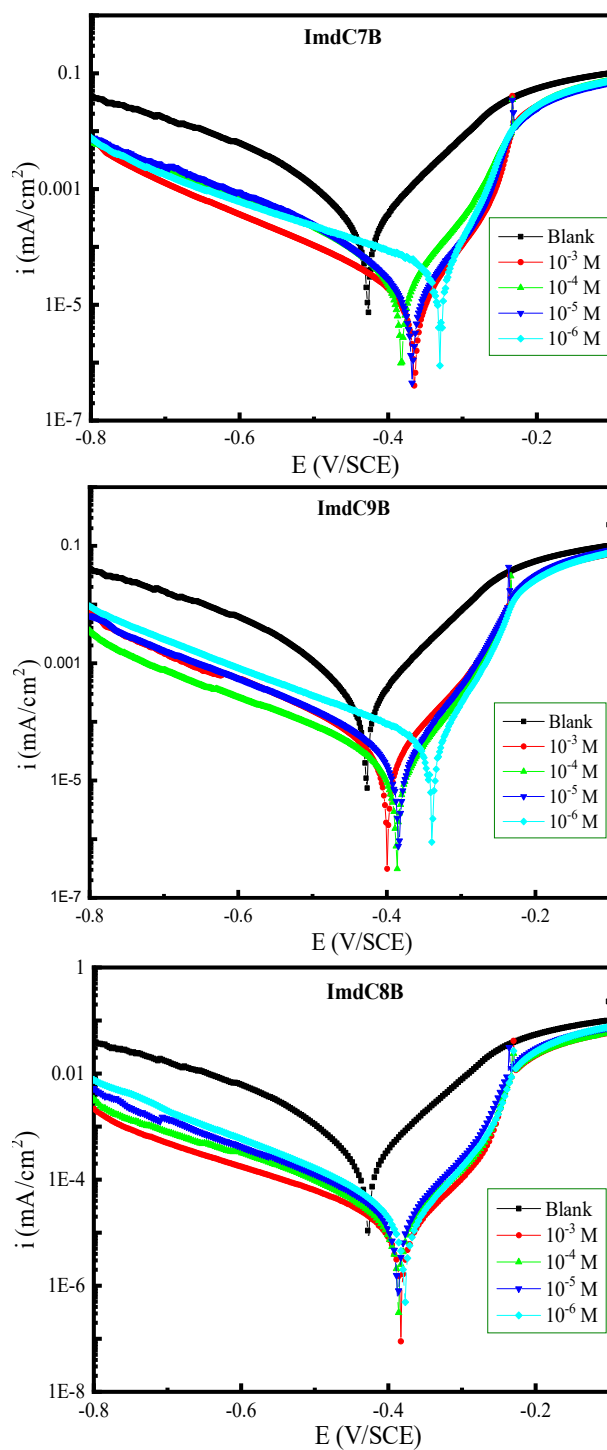


Fig. 1. Polarization curves of the MS recorded after 30 min of immersion, at 303 K in 1 M HCl containing different concentrations of ImdC7B, ImdC8B and ImdC9B

3.2. EIS

In order to better understand the mode of action of these corrosion inhibitors, we studied their behavior through the electrochemical impedance spectroscopy technique; several studies have been carried out to determine the reaction mechanisms (charge transfer, diffusion, adsorption, etc.) exploiting this technique [38-40]. The Nyquist diagrams of steel immersed in acid solutions without and with the addition of different concentrations for ImdC7B, ImdC8B and ImdC9B are presented in Figure2.

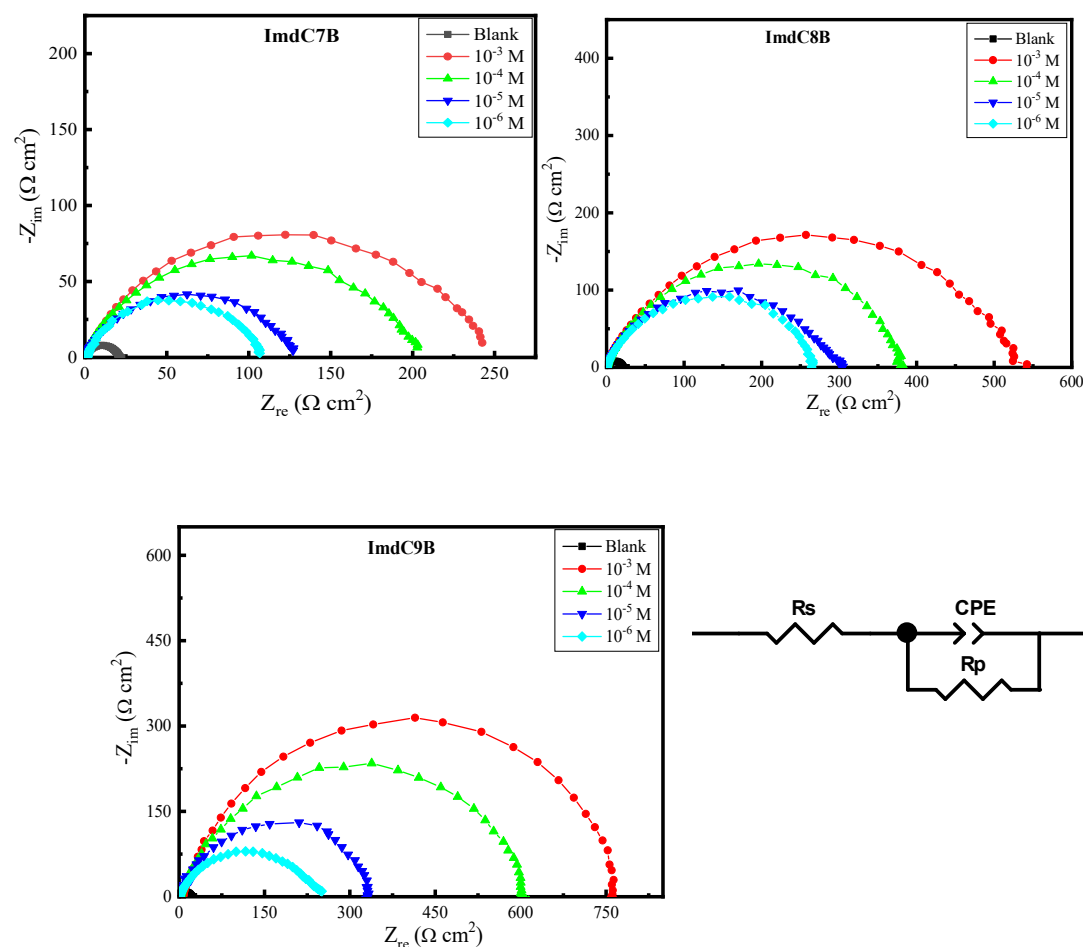


Fig. 2. Nyquist plots of steel in 1 M HCl with and without ImdC7B, ImdC8B and ImdC9B at 303 K, and the relevant equivalent circuit

Nyquist diagrams illustrate capacitive loops (semicircle) whose center is below the abscissa axis. The phase difference noted between the ideal case and the impedance diagrams obtained in our study has been attributed to the frequency dispersion in the majority of works [41,42] as well as to various physical phenomena such as roughness and non-homogeneity of the surface. They indicate that the corrosion of steel in the absence and in the presence of inhibitor is

controlled by a charge transfer process [43], the increase in the concentrations of organic compounds in the HCl (1M) medium produces a change in the shape and size of the diagrams, which have a similar shape for all the concentrations tested, indicating that almost there is no change in the corrosion mechanism. In low frequencies, the impedance behavior is linked to the adsorption of inhibitors on the metal surface and the accumulation of all other species on the metal / solution interface (inhibitors, corrosion products, etc.) [44].

Electrochemical parameters have been obtained employing fitting tool of ZView 2.80 software. Otherwise, the χ^2 has been exploited to find the model best suited to our system, the very low values of χ^2 ($\approx 1 \times 10^{-3}$) illustrated in Table 3 allowed us to say that there has a very good correlation between the simulated curves and the experimental curves obtained in this study. The values of the parameters associated with these measurements and extracted from the circuit of Figure 2 adopted in this study (resistance, capacity, inhibition performance...) are collated in Table 3. Following these various observations, the electrochemical interface metal/electrolyte is equivalent to an electrical circuit consisting of a polarization resistance R_p in parallel with a constant phase element (CPE), the assembly is in series with the solution resistance (R_s) as shown in Figure 2. This resistance R_p include in addition to the resistance of the inhibitor film (R_f) the resistance to charge transfer (R_{ct}) ($R_p = R_f + R_{ct}$) [45]. The utilize of such a CPE instead of a capacitor explains the deviations from the ideal dielectric behavior, and is linked to the inhomogeneities of the surface which causes greater depression in the semicircular form of Nyquist [46,47]. The impedance, Z , of the CPE is given by the formula [42]:

$$Z_{CPE} = \frac{1}{Q(i\omega)^n} \quad (3)$$

Where Q is the CPE modulus, ω is called the angular frequency; i is the imaginary roots and n is may be employed as an indicator of the surface homogeneity. When $n = +1$, -1 or 0 , CPE depicts pure capacitor, inductor or resistor, respectively. The values of C_{dl} were estimated through the next formula [42]:

$$C_{dl} = (Q^{1/n} R_p^{1-n/n}) \quad (4)$$

From Table 3, we note that when the concentration of ImdC7B, ImdC8B and ImdC9B reduces, the Q values decrease, this can be explained by the increase in the quantity of ImdC7B, ImdC8B and ImdC9B molecules adsorbed on the surface of MS. Nevertheless, the values of phase change (n) tend to move towards unity due to the changes in the homogeneity of the solution and also due to the changes taking place at metal/solution interface. This phenomenon can be correlated to the surface assimilation of ImdC7B, ImdC8B and ImdC9B molecules on MS that mitigates the penetration of corrosive media [48].

Table 3. Impedance parameters of MS in 1 M HCl with and without ImdC7B, ImdC8B and ImdC9B at 303 K.

Medium	Conc. (mM)	R _s (Ω cm ²)	R _p (Ω cm ²)	CPE		C _{dl} (μF cm ⁻²)	χ × 10 ⁻³	P _{EIS} (%)
				Q × 10 ⁵ (μF S ⁿ cm ⁻²)	n			
Blank	—	0.66±0.02	23.0±0.2	29.38±0.12	0.897±0.003	165.5	5.0	—
ImdC7B	10 ⁻³	1.22±0.01	240.2±2.1	12.24±0.10	0.768±0.003	42.2	1.2	90.4
	10 ⁻⁴	1.25±0.02	204.6±3.1	13.02±0.09	0.832±0.008	62.6	3.1	88.8
	10 ⁻⁵	0.96±0.02	128.3±1.2	15.16±0.09	0.844±0.005	73.2	3.6	82.1
	10 ⁻⁶	1.19±0.01	102.8±1.1	18.18±0.07	0.857±0.004	93.9	1.8	77.6
ImdC8B	10 ⁻³	1.22±0.03	534.4±3.5	06.21±0.02	0.822±0.005	29.7	4.0	95.7
	10 ⁻⁴	1.82±0.03	384.3±3.0	08.47±0.01	0.828±0.008	41.6	2.8	94.0
	10 ⁻⁵	1.30±0.02	307.0±2.4	10.83±0.02	0.822±0.004	51.8	3.2	92.5
	10 ⁻⁶	1.82±0.03	260.8±1.5	18.02±0.03	0.832±0.004	97.2	2.9	91.2
ImdC9B	10 ⁻³	2.62±0.01	751.6±4.4	05.92±0.02	0.846±0.003	33.6	0.8	96.9
	10 ⁻⁴	2.55±0.01	611.8±3.5	07.77±0.01	0.828±0.004	41.3	4.0	96.2
	10 ⁻⁵	1.89±0.03	327.4±3.6	08.81±0.02	0.856±0.003	48.5	3.2	93.0
	10 ⁻⁶	1.01±0.02	248.9±2.3	12.55±0.03	0.858±0.003	70.7	2.0	90.7

3.3. Determination of the adsorption isotherm and thermodynamic parameters

The inhibition of corrosion of metals by organic compounds is explained by their adsorption on the metal surface. The adsorption isotherms are then an important complement capable of determining the electrochemical mechanism which leads to the adsorption of these organic compounds on the surface. In order to obtain the type of adsorption corresponding to our study, we plotted the C_{inh}/θ as a function of the concentration of ImdC7B, ImdC8B and ImdC9B. Figure 3 represents the adsorption isotherm of ImdC7B, ImdC8B and ImdC9B. The recovery rate of the metal surface is related to the concentration of the inhibitor by the following relationship [49]:

$$C_{inh} \times \theta^{-1} = (K_{ads})^{-1} + C_{inh} \quad (5)$$

In the equation, C_{inh} is the concentration of ImdC7B, ImdC8B and ImdC9B. K_{ads} is the adsorption equilibrium constant and θ is the surface coverage area governs by ImdC7B, ImdC8B and ImdC9B. The degree of surface coverage (θ) was evaluated from the polarization curves technique and the values of this parameter are gathered in the Table 2. The plot of the Langmuir adsorption isotherm obtained from equation 5 and the values given in Table 4 is given in Figure 3.

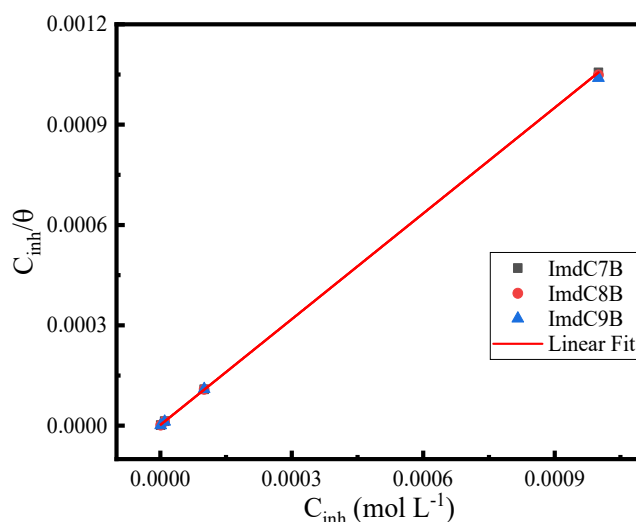


Fig. 3. Isothermal adsorption of ImdC7B, ImdC8B and ImdC9B on MS in 1 M HCl at 303 K

Table 4. Langmuir isotherm adsorption parameters for MS in 1 M HCl containing ImdC7B, ImdC8B and ImdC9B at 303 K.

Inhibitors	R ²	Slopes	K _{ads} (L/mol)	ΔG _{ads} [°] (KJ/mol)
ImdC7B	1.0000	1.05	4.59×10 ⁵	-42.96
ImdC8B	1.0000	1.05	4.57×10 ⁵	-42.95
ImdC9B	0.99999	1.04	4.24×10 ⁵	-42.76

Upon adsorption of any component in the metal / electrolyte interphase, new forces of attraction appear. As a result, all adsorptions are generally accompanied by a release of energy. The standard free enthalpy of adsorption (ΔG_{ads}[°]) and the adsorption constant (K_{ads}) are connected by equation (6)[50-52]:

$$\Delta G_{ads}^{\circ} = -R \times T \times \ln(55.5 \times K_{ads}) \quad (6)$$

55.5 is the concentration of water in the solution expressed by mol/L, R is the gas constant and T is the absolute temperature.

The values obtained from ΔG_{ads}[°] is negative and the value of K_{ads} is very high which reveals to adsorption of a ImdC7B, ImdC8B and ImdC9B compounds strongly on the surface of MS and demonstrate the adsorbed layer stability on the surface of MS. In general, when the results of free energy of adsorption reach to -20 KJ mol⁻¹ this reveal to the electrostatic reaction between the charged metal and inhibitor charged molecules, and this relation was named by physical adsorption. But when the values of free energy adsorption more negative than -40 KJ mol⁻¹, this include transfer or contribution of the electrons from the molecules of the inhibitor

on the surface of the metal to give a coordination bond and this relation was named by chemical adsorption [53]. The free energy adsorption values, which gained were about equal to -43 KJ mol^{-1} for the three tested compounds (Table 4), and this assured that the mechanism of adsorption of ImdC7B, ImdC8B and ImdC9B on MS-substrate surface in a 1 M HCl solution, includes chemical adsorption [54].

3.4. Quantum chemical computation method

In order to follow the influence of the carbon chain on the electronic behavior of the benzimidazolium bromide (ImdC7B, ImdC8B and ImdC9B), we exploited the quantum chemical computation method. The geometrical relaxation of these cationic forms is carried out after the optimization process by the DFT concept. The optimized molecular geometry and the of FMO (HOMO and LUMO) electron densities of the benzimidazolium bromide series is illustrated in Figures 4 and 5, respectively. The optimized structures (Figure 4) of the investigated ion forms show no negative frequencies, which indicates that the special geometry of these forms is quite stable. As appeared in Figure 5, the LUMO electron densities are located on the molecular skeleton of benzimidazolium for the three ionic compounds. This presents that all atoms within this zone are ready to receive the electrons for the ImdC7B, ImdC8B and ImdC9B species. Though, the electron density distribution of HOMO varies from one molecule to another in our series. This behavior is probably due to the influence of the increase of the carbon chain from C8 to C9. The regions occupied by the HOMO density are considered as electron donor units to the lacunae found in the metal surface of the iron. All regions occupied by FMO densities present the molecular reactivity of the species studied, hence the appearance of the corrosion-inhibitory property of MS-substrate. In addition, we can see that this characteristic makes it possible to predict the mode of adsorption of these ionic forms on the metal surface.

E_{HOMO} and E_{LUMO} are the critical descriptors to calculate the adsorption level of an inhibitor molecule on the metal steel [55]. In the light of the data outlined in Table 5, it is evident that the E_{HOMO} of the ImdC9B is higher than that of the ImdC7B and ImdC8B. It strongly suggests that the molecule with C10 in the carbon chain has the greatest propensity to send electrons to the metallic surface. Hence, the results consolidated in Table 5 reveal that the ImdC9B provides the lowest value of the ΔE_{gap} , which is a confirmation of the highest reactivity with the metallic surface. The literature demonstrates that the difference in electronegativity (χ) behaves like the thrust such that the transfer of charge occurs between two atoms, which must transfer through the global hardness (η) which acts as a resistance in the movement of electrons [56].

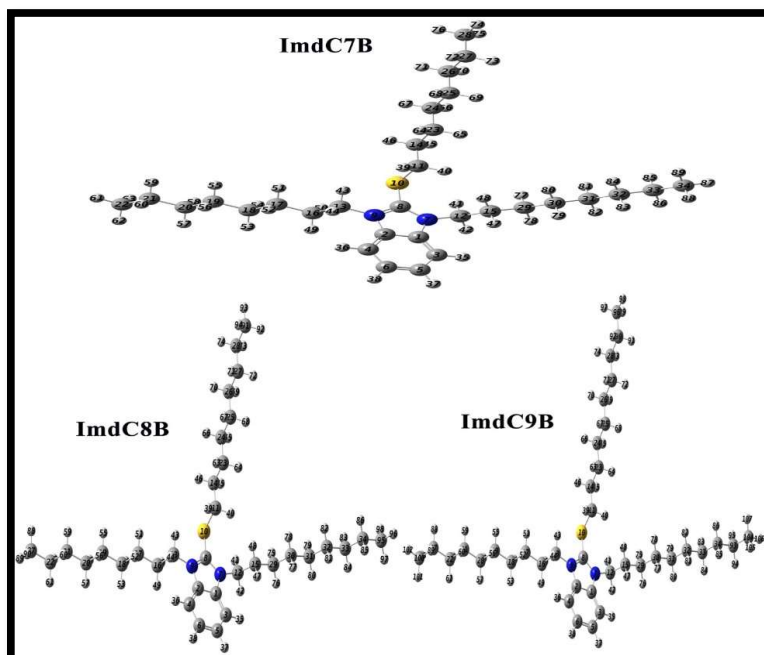


Fig. 4. Optimized structures of ImdC7B, ImdC8B and ImdC9B

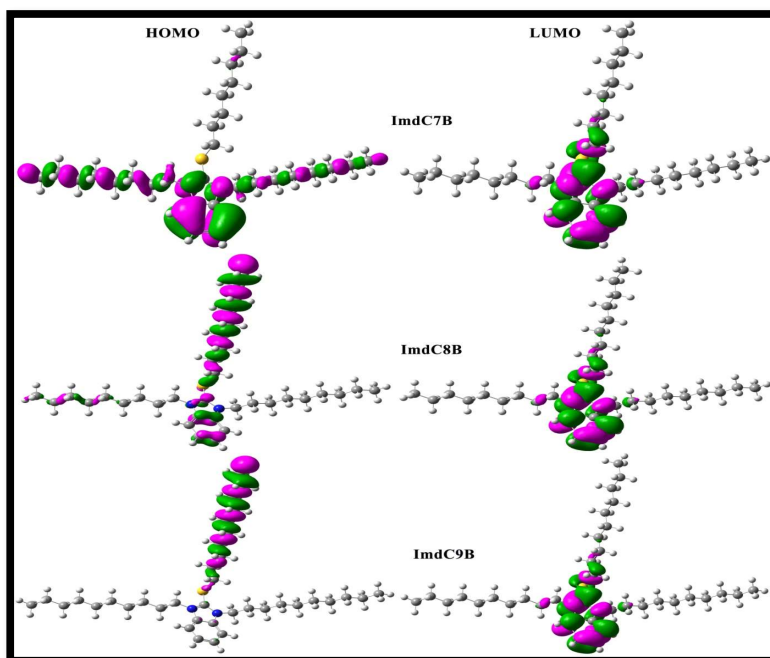


Fig. 5. HOMO/ LUMO distributions of ImdC7B, ImdC8B and ImdC9B

χ and η were significantly smaller for ImdC9B than for the ImdC7B and ImdC8B cationic forms. This implies that this compound (ImdC9B) has a stronger potential to absorb on the

steel surface. The fraction of transmitted electrons (ΔN_{110}) was the largest in the case of ImdC9B, supporting the greatest preference for the donation of electrons. A high value of this descriptor indicates a high chemical reactivity [57]. Dipolar moment (μ) is another descriptor exploited to evaluate the reactivity of a molecule [58]. A high value of this descriptor indicates a high chemical reactivity. In our case, de compound ImdC9B validates this property.

All the calculation results obtained confirm the order of inhibitory efficacy $\text{ImdC7B} < \text{ImdC8B} < \text{ImdC9B}$, the improvement in the linear carbon chain thus contributes to an increase in chemical reactivity.

Table 5. DFT calculated descriptors of benzimidazolium bromide, ImdC7B, ImdC8B and ImdC9B.

Benzimidazolium bromide	E_{HOMO} (eV)	E_{LUMO} (eV)	ΔE_{gap} (eV)	χ (eV)	η (eV)	ΔN_{110}	μ (D)
ImdC7B	-10.183	-5.230	4.953	7.7065	2.4765	-0.583	7.346
ImdC8B	-10.027	-5.221	4.806	7.624	2.403	-0.583	8.295
ImdC9B	-9.826	-5.219	4.607	7.5225	2.3035	-0.587	9.465

Active local centres located in benzimidazolium bromide, ImdC7B, ImdC8B and ImdC9B, are determined exploiting the Fukui functions which are computed via the DMol³ module introduced in the Materials Studio package (Ver. 8.0) [59]. In this study, the Generalized Gradient Approximation (GGA) of the Perdew-Burke-Ernzerh of (PBE) formula was exploited for the electron exchange potential-electron correlation, and the all-electron calculations were carried out with a double numerical basis (DNP).

The Fukui functions allow to find the reactive sites that are directly responsible on the electrophilic (f_k^-) and nucleophilic (f_k^+) attacks of the ImdC7B, ImdC8B and ImdC9B. We accept that the most condensed functions contain the most reactive sites with the metal surface [60].

The two Fukui functions are calculated and determined exploiting the following two equations:

$$\text{➤ Nucleophilic attack} \rightarrow f_k^+ = P_k(N+1) - P_k(N) \quad (7)$$

$$\text{➤ Electrophilic attack} \rightarrow f_k^- = P_k(N) - P_k(N-1) \quad (8)$$

where $P_k(N)$, $P_k(N+1)$ and $P_k(N-1)$ are the neutral, anionic and cationic of the molecule, respectively.

Table 6 presents the values of the Fukui functions for the two electrophilic and nucleophilic attacks of the cationic forms investigated. The comprehensive analysis of the results shows that these forms present a majority property of accepting electrons from the donor centres located in the metallic surface of the iron. The most favourable atoms to receive electrons for the three cationic forms are C (3), C (4), C (5), C (6), N (7) and C (8). These atoms are responsible for

the molecular reactivity, indicating a considerable inhibitory efficacy against MS-substrate corrosion. The electron donor effect is almost absent for the three species studied, due to the protonated (cationic) form which normally blocks the release of electrons towards empty orbitals.

Table 6. Fukui functions of ImdC7B, ImdC8B and ImdC9B calculated at the DFT/GGA/DNP level

Atoms	f_k^-	f_k^+	f_k^-	f_k^+	f_k^-	f_k^+
C (1)	0.004	0.016	0.002	0.014	0.002	0.013
C (2)	0.005	0.016	0.000	0.017	0.000	0.017
C (3)	0.015	0.053	0.007	0.040	0.006	0.040
C (4)	0.013	0.053	0.001	0.033	0.001	0.033
C (5)	0.019	0.053	0.009	0.045	0.008	0.045
C (6)	0.012	0.053	0.008	0.054	0.007	0.054
N (7)	0.007	0.045	0.005	0.059	0.005	0.059
C (8)	0.003	0.092	0.001	0.098	0.002	0.097
N (9)	0.009	0.045	0.001	0.056	0.001	0.055
S (10)	0.012	0.102	0.002	0.084	0.001	0.084
C (11)	0.003	0.034	0.002	0.022	0.001	0.022
C (12)	0.003	0.008	0.001	0.011	0.001	0.011
C (13)	0.005	0.007	0.003	0.013	0.002	0.013
C (14)	0.006	0.009	0.004	0.008	0.003	0.008
C (15)	0.003	0.004	0.001	0.005	0.000	0.005
C (16)	0.007	0.004	0.005	0.006	0.003	0.006
C (17)	0.010	0.004	0.007	0.005	0.005	0.005
C (18)	0.015	0.002	0.013	0.004	0.010	0.004
C (19)	0.018	0.002	0.021	0.003	0.015	0.003
C (20)	0.027	0.001	0.025	0.002	0.020	0.002
C (21)	0.026	0.002	0.033	0.001	0.020	0.001
C (22)	0.028	0.003	0.036	0.001	0.034	0.001
C (23)	0.010	0.006	0.008	0.006	0.007	0.006
C (24)	0.016	0.004	0.013	0.005	0.012	0.005
C (25)	0.020	0.002	0.020	0.003	0.020	0.003
C (26)	0.031	0.002	0.026	0.002	0.023	0.002
C (27)	0.030	0.002	0.031	0.002	0.032	0.001
C (28)	0.032	0.003	0.028	0.002	0.034	0.001
C (29)	0.004	0.004	0.001	0.005	0.001	0.005
C (30)	0.007	0.002	0.000	0.003	0.000	0.003
C (31)	0.008	0.002	0.001	0.003	0.000	0.003
C (32)	0.012	0.001	0.000	0.001	0.000	0.001
C (33)	0.012	0.002	0.001	0.002	0.000	0.002
C (34)	0.014	0.001	0.001	0.002	0.000	0.002
C (87)			0.001	0.001	0.001	0.002
C (88)			0.002	0.002	0.002	0.002
C (89)			0.003	0.001	0.003	0.003
C (99)					0.000	0.003
C (100)					0.000	0.003
C (101)					0.000	0.001

3.5. MD simulation analysis

Molecular dynamics (MD) simulation allows us to try to understand the behavior and configurationally change in the structure of the inhibitor molecules when they come into contact with the steel surface in order to perform adsorption mode analysis [61-63]. Figure 6 illustrates the final adsorption configuration of the cationic forms ImdC7B, ImdC8B and ImdC9B on the Fe (110) surface. During the simulation, the investigated cationic forms shift towards the ferrous surface under the effect of the attractive forces in order to eliminate the water layer. This shows that the adsorption of the species studied is parallel with the first layer of iron atoms. This implies a high degree of interaction. This indicates that the physical interactions are taken into account [64]; we could easily surmise that ImdC9B compound would be the better inhibitor than ImdC7B and ImdC8B.

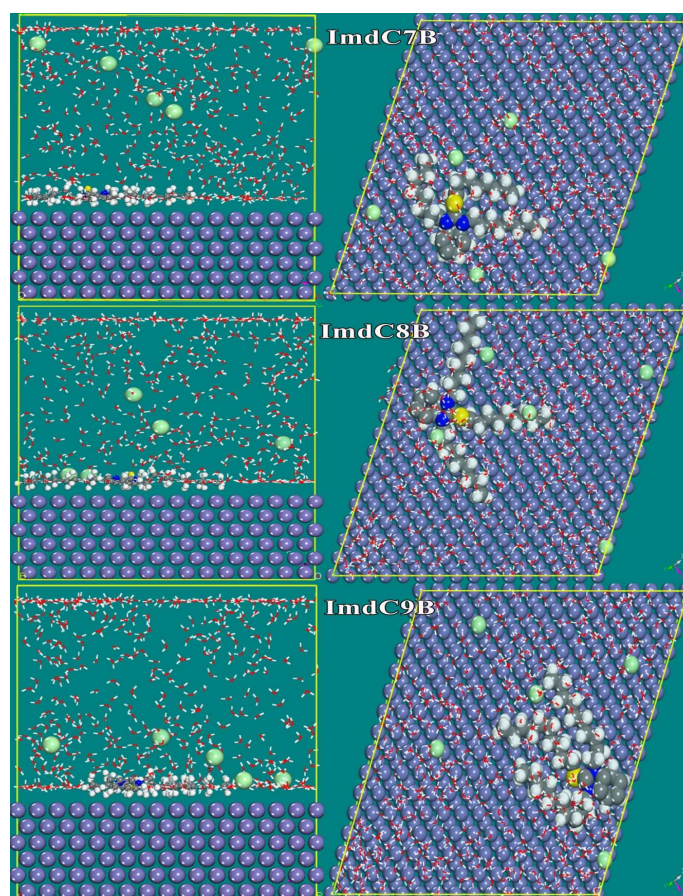


Fig. 6. Side (left) and top (right) views of the equilibrium adsorption configurations of ImdC7B, ImdC8B and ImdC9B on the Fe (110) surface in HCl.

The energy values, namely $E_{\text{interaction}}$ and E_{binding} of the simulated system (inhibitory species-Fe (110)) are given in Table 7. After examination of the results of this table, it can be

seen that the negative values of $E_{\text{interaction}}$ of three simulated systems indicate the spontaneity of the interaction process [65]. The more negative value of $E_{\text{interaction}}$ (-861.458 kJ/mol) and the more positive value of E_{binding} (861.458 kJ/mol) of ImdC9B indicates that this compound interacts and adsorbs more efficiently on the steel surface than ImdC7B and ImdC8B [66]. These simulation results show that the adsorption performance of the cationic forms on the iron surface increases in the following sequence: ImdC7B < ImdC8B < ImdC9B. This classification is the same as who got through the experience. Therefore, it can be concluded that the increase of the carbon chain has a positive influence on the adsorption performance of the protonated molecules on the iron surface, resulting in a better corrosion protection efficiency of the steel [67].

Table 7. Calculated quantum chemical descriptors for ImdC7B, ImdC8B and ImdC9B

Systems	$E_{\text{interaction}}$ (kJ/mol)	E_{binding} (kJ/mol)
ImdC7B-Fe(110)	-839.821	839.821
ImdC8B-Fe(110)	-856.670	856.670
ImdC9B-Fe(110)	-861.458	861.458

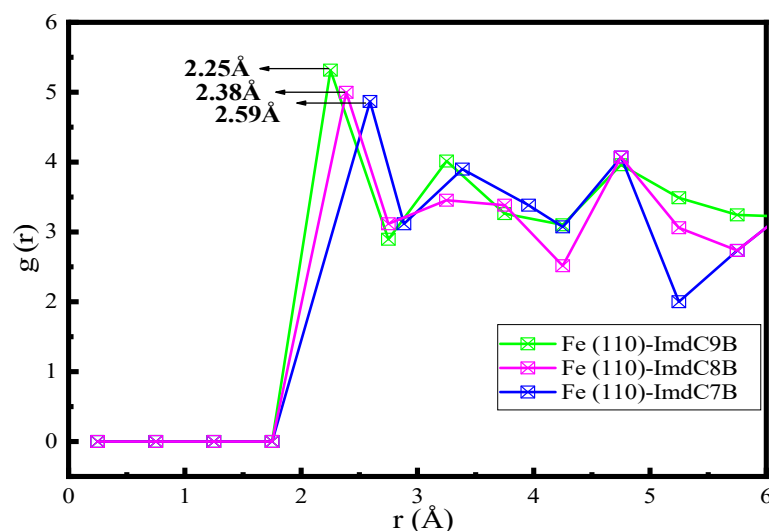


Fig. 7. RDF of ImdC7B, ImdC8B and ImdC9B on the Fe (110) surface at 303 K

The adsorption of inhibitor compounds on the metallic surface is largely dependent of the types of bonds that are formed between them [68]. The radial distribution function (RDF) method concentrates on the structural assessment of the MD simulation results and has been applied to reveal the type of chemical and physical bonds [69]. Figure 7 shows that the observed values at the first peak for each bond length of the adsorption of the cationic forms ImdC7B, ImdC8B and ImdC9B on the Fe (110) surface at the simulated temperature of 303 K are within

the chemisorption range (1-3.5Å) [70]. These results prove that the species studied adsorb efficiently on the metal surface by coordination bonds.

4. CONCLUSION

The present work relates to the study of the inhibition of corrosion of MS-substrate by organic compounds of benzimidazolium type in a 1 M HCl medium. The results obtained in this study showed that the inhibitory efficacy increases with increasing concentration of inhibitor. The best inhibitor in this series is the compound ImdC9B with an efficiency which can reach up to 96.9% at 10^{-3} M. The adsorption of all the organic inhibitors tested in this work follows the Langmuir isotherm model. The polarization curves show that the inhibitors tested are inhibitors predominantly anodic. The impedance measurements show that the polarization resistances increase with the increase in the concentration of each inhibitor, on the other hand, the double layer capacity decreases due to the adsorption of the compounds on the steel surface thanks to the formation of a protective layer of the acid solution. The theoretical approaches exploited support the experimental results well.

REFERENCES

- [1] A. Zarrouk, B. Hammouti, T. Lakhlifi, M. Traisnel, H. Vezin, and F. Bentiss, *Corros. Sci.* 90 (2015) 572.
- [2] L. Fragoza-Mar, O. Olivares-Xometl, M. A. Domínguez-Aguilar, E. A. Flores, P. Arellanes-Lozada, and F. Jiménez-Cruz, *Corros. Sci.* 61 (2012) 171.
- [3] M. Belayachi, H. Serrar, H. Zarrok, A. El Assyry, A. Zarrouk, H. Oudda, S. Boukhris, B. Hammouti, Eno E. Ebenso, and A. Geunbour, *Int. J. Electrochem. Sci.* 10 (2015) 3010.
- [4] H. Zarrok, A. Zarrouk, R. Salghi, Y. Ramli, B. Hammouti, M. Assouag, E. M. Essassi, H. Oudda, and M. Taleb, *J. Chem. Pharm. Res.* 4 (2012) 5048.
- [5] A. Zarrouk, B. Hammouti, H. Zarrok, R. Salghi, A. Dafali, L. h. Bazzi, L. Bammou, and S. S. Al-Deyab, *Der Pharma Chem.* 4 (2012) 337.
- [6] H. Zarrok, K. Al Mamari, A. Zarrouk, R. Salghi, B. Hammouti, S. S. Al-Deyab, E. M. Essassi, F. Bentiss, and H. Oudda, *Int. J. Electrochem. Sci.* 7 (2012) 10338.
- [7] N. Anusuya, J. Saranya, P. Sounthari, A. Zarrouk, and S. Chitra, *J. Mol. Liq.* 225 (2017) 406.
- [8] M. Lebrini, M. Lagrenée, H. Vezin, M. Traisnel, and F. Bentiss, *Corros. Sci.* 49 (2007) 2254.
- [9] M. El Hezzat, M. Assouag, H. Zarrok, Z. Benzekri, A. El Assyry, S. Boukhris, A. Souizi, M. Galai, R. Touir, M. Ebn Touhami, H. Oudda, and A. Zarrouk, *Der Pharma Chem.* 7 (2015) 77.

- [10] D. Ben Hmamou, M. R. Aouad, R. Salghi, A. Zarrouk, M. Assouag, O. Benali, M. Messali, H. Zarrok, and B. Hammouti, *J. Chem. Pharm. Res.* 4 (2012) 3489.
- [11] F. Bentiss, M. Traisnel, and M. Lagrenée, *Corros. Sci.* 42 (2000) 127.
- [12] A. Zarrouk, M. Messali, M. R. Aouad, M. Assouag, H. Zarrok, R. Salghi, B. Hammouti, and A. Chetouani, *J. Chem. Pharm. Res.* 4 (2012) 3427.
- [13] A. Dehghani, G. Bahlakeh, B. Ramezanzadeh, and M. Ramezanzadeh, *J. Mol. Liq.* 298 (2020) 112046.
- [14] D. Ben Hmamou, R. Salghi, A. Zarrouk, H. Zarrok, B. Hammouti, S. S. Al-Deyab, M. Bouachrine, A. Chakir, and M. Zougagh, *Int. J. Electrochem. Sci.* 7 (2012) 5716.
- [15] Y. ELouadi, F. Abridgach, A. Bouyanzer, R. Touzani, O. Riant, B. ElMahi, A. El Assyry, S. Radi, A. Zarrouk, and B. Hammouti, *Der Pharma Chem.* 7 (2015) 265.
- [16] A. Dehghani, G. Bahlakeh, B. Ramezanzadeh, and M. Ramezanzadeh, *Constr. Build. Mater.* 245 (2020) 118464.
- [17] S. A. Umoren, and M. M. Solomon, *J. Environ. Chem. Eng.* 5 (2017) 246.
- [18] R. Tourir, R. A. Belakhmima, M. Ebn Touhami, L. Lakhrissi, M. El Fayed, B. Lakhrissi, and E. M. Essassi, *J. Mater. Environ. Sci.* 4 (2013) 921.
- [19] X. Wang, H. Yang, and F. Wang, *Corros. Sci.* 53 (2011) 113.
- [20] F. Zhang, Y. Tang, Z. Cao, W. Jing, and Z. Wu, *Corros. Sci.* 8 (2012) 378.
- [21] H. J. Guadalupe, E. García-Ochoa, P. J. Maldonado-Rivas, J. Cruz, and T. Pandiyan, *J. Electroanal. Chem.* 655 (2011) 164.
- [22] K. Ansari, D. S. Chauhan, M. Quraishi, M. A. Mazumder, and A. Singh, *Int. J. Biol. Macromol.* 144 (2020) 305.
- [23] X. Luo, C. Ci, J. Li, K. Lin, S. Du, H. Zhang, X. Li, Y. F. Cheng, J. Zang, and Y. Liu, *Corros. Sci.* 151 (2019) 132.
- [24] F. Benhiba, H. Zarrok, A. Elmidaoui, M. El Hezzate, R. Tourir, A. Guenbour, A. Zarrouk, S. Boukhris, and H. Oudda, *J. Mater. Environ. Sci.* 6 (2015) 2301.
- [25] B. Tana, S. Zhang, H. Liu, Y. Qiang, W. Li, L. Guo d, and S. Chen, *J. Taiwan. Inst. Chem. E* 102 (2019) 424.
- [26] M. Frisch, G. Trucks, H. B. Schlegel, G. Scuseria, M. Robb, J. Cheeseman, G. Scalmani, V. Barone, B. Mennucci, and G. Petersson, *Gaussian 09, revision D. 01*, Gaussian, Inc., Wallingford CT, 2009.
- [27] A. El Assyry, M. Touil, F. Benhiba, B. Benali, H. Rabaâ, B. Lakhrissi, I. Warad, F. Bentiss, and A. Zarrouk, *Anal. Bioanal. Electrochem.* 12 (2020) 580.
- [28] F. Benhiba, H. Serrar, R. Hsissou, A. Guenbour, A. Bellaouchou, M. Tabyaoui, S. Boukhris, H. Oudda, I. Warad, and A. Zarrouk, *Chem. Phys. Lett.* 743 (2020) 137181.
- [29] T. Laabaissi, F. Benhiba, M. Missioui, Z. Rouifi, M. Rbaa, H. Oudda, Y. Ramli, A. Guenbour, I. Warad, and A. Zarrouk, *Heliyon* 6 (2020) e03939.
- [30] Materials Studio, Revision 8.0, Accelrys Inc., San Diego, USA (2015).

- [31] H. Sun, COMPASS: J. Phys. Chem. B 102 (1998) 7338.
- [32] H.C. Andersen, J. Chem. Phys. 72 (1980) 2384.
- [33] M. Farsak, H. Keleş, and M. Keleş, Corros. Sci. 98 (2015) 223.
- [34] A. Salhi, S. Tighadouini, M. El-Massaoudi, M. Elbelghiti, A. Bouyanzer, S. Radi, S. El Barkany, F. Bentiss, and A. Zarrouk, J. Mol. Liq. 248 (2017) 340.
- [35] H. Ouici, M. Tourabi, O. Benali, C. Selles, C. Jama, A. Zarrouk, and F. Bentiss, J. Electroanal. Chem. 803 (2017) 125.
- [36] F. Z. Bouanis, F. Bentiss, M. Traisnel, and C. Jama, Electrochim. Acta 54 (2009) 2371.
- [37] O. Olivares-Xometl, E. Álvarez-Álvarez, N. V. Likhanova, I. V. Lijanov, R. E. Hernández-Ramírez, P. Arellanes-Lozada, and J. L. Varela-Caselis, J. Adhes. Sci. Technol. 32 (2018) 1092.
- [38] A. Khadraoui, A. Khelifa, M. Hadjmeliani, R. Mehdaou, K. Hachama, A. Tidu, Z. Azari, I.B. Obot, and A. Zarrouk, J. Mol. Liq. 216 (2016) 724.
- [39] A. Tazouti, M. Galai, R. Tourir, M. Ebn Touhami, A. Zarrouk, Y. Ramli, M. Saraçoğlu, S. Kaya, F. Kandemirli, and C. Kaya, J. Mol. Liq. 221 (2016) 815.
- [40] A. E. Stoyanova, E. I. Sokolova, and S. N. Raicheva, Corros. Sci. 39 (1997) 1595.
- [41] S. Martinez, and M. Metikos-Hukovic, J. Appl. Electrochem. 33 (2003) 1137.
- [42] Y. Kharbach, F. Z. Qachchachi, A. Haoudi, M. Tourabi, A. Zarrouk, C. Jama, L. O. Olasunkanmi, E. E. Ebenso, and F. Bentiss, J. Mol. Liq. 246 (2017) 302.
- [43] H. Vashisht, S. Kumar, I. Bahadur, and G. Singh, Int. J. Electrochem. Sci. 8 (2013) 684.
- [44] M. Erbil, Chim. Acta Turc. 1 (1988) 59.
- [45] M. El Faydy, R. Tourir, M. Ebn Touhami, A. Zarrouk, C. Jama, B. Lakhrissi, L. O. Olasunkanmi, E. E. Ebenso, and F. Bentiss, Phys. Chem. Chem. Phys. 20 (2018) 20167.
- [46] V. F. Lvovich, Impedance Spectroscopy: Applications to Electrochemical and Dielectric Phenomena: Wiley, 2015.
- [47] E. Barsoukov, and J. R. Macdonald, Impedance Spectroscopy: Theory, Experiment, and Applications: Wiley, 2005.
- [48] Q. Zhou, S. Sheikh, P. Ou, D. Chen, and S. Guo, Electrochem. Commun. 98 (2019) 63.
- [49] M. El Faydy, M. Galai, M. Ebn Touhami, I. B. Obot, B. Lakhrissi, and A. Zarrouk, J. Mol. Liq. 248 (2017) 1014.
- [50] S. S. Abd El Rehim, S. M. Sayyah, M. M. El-Deeb, S. M. Kamal, and R. E. Azooz, Int. J. Ind. Chem. 7 (2016) 39.
- [51] H. S. Gadow, and M. M. Motawea, RSC Adv. 7 (2017) 24576.
- [52] I. Hamdani, E. El Ouariachi, O. Mokhtari, A. Salhi, N. Chahboun, B. ElMahi, A. Bouyanzer, A. Zarrouk, and B. Hammouti, J. Costa, Der Pharma Chem. 7 (2015) 252.
- [53] F. El-Taib Heakal, M. A. Deyab, M. M. Osman, M. I. Nessim, and A. E. Elkholy, RSC Adv. 7 (2017) 47335.

- [54] M. El Faydy, M. Rbaa, L. Lakhrissi, B. Lakhrissi, I. Warad, A. Zarrouk, and I. B. Obot, *Surf. Interfaces* 14 (2019) 222.
- [55] F. Benhiba, R. Hsissou, Z. Benzekri, M. E. Belghiti, A. Lamhamdi, A. Bellaouchou, A. Guenbour, S. Boukhris, H. Oudda, I. Warad, and A. Zarrouk, *J. Mol. Liq.* 312 (2020) 113367.
- [56] M. Murmu, S. K. Saha, N.C. Murmu, and P. Banerjee, *Corros.Sci.* 146 (2019) 134.
- [57] F. Benhiba, Z. Benzekri, A. Guenbour, M. Tabyaoui, A. Bellaouchou, S. Boukhris, H. Oudda, I. Warad, and A. Zarrouk, *Chin. J. Chem. Eng.* 28 (2020) 1436.
- [58] J. Haque, C. Verma, V. Srivastava, M. A. Quraishi, and E. E. Ebenso, *Results Phys.* 9 (2018) 1481.
- [59] A. Elbarki, W. Guerrab, T. Laabaissi, F. Benhiba, Z. Rouifi, H. Oudda, A. Guenbour, R. Touri, I. Warad, Y. Ramli, and A. Zarrouk, *Chem. Data Collect.* 28 (2020) 100454.
- [60] E. Ech chihbi, A. Nahlé, R. Salim, F. Benhiba, A. Moussaif, F. El-Hajjaji, H. Oudda, A. Guenbour, M. Taleb, I. Warad, and A. Zarrouk, *J. Alloy. Compd.* (2020)155842. <https://doi.org/10.1016/j.jallcom.2020.155842>.
- [61] M. El Faydy, H. About, F. Benhiba, B. Lakhrissi, A. Guenbour, F. Bentiss, I. Warad, E. E. Ebenso, and A. Zarrouk, *Surf. Interfaces* 20 (2020) 100575.
- [62] E. Alibakhshi, M. Ramezanzadeh, G. Bahlakeh, B. Ramezanzadeh, M. Mahdavian, and M. Motamedi, *J. Mol. Liq.* 255 (2018) 185.
- [63] A. Berrissoul, A. Ouarhach, F. Benhiba, A. Romane, A. Zarrouk, A. Guenbour, B. Dikici, and A. Dafali, *J. Mol. Liq.* 313(2020)113493.
- [64] S.-W. Xie, Z. Liu, G.-C. Han, W. Li, J. Liu, and Z. Chen, *Comput. Theor. Chem.* 1063 (2015) 50.
- [65] Z. Rouifi, M. Rbaa, Ashraf S. Abousalem, F. Benhiba, T. Laabaissi, H. Oudda, B. Lakhrissi, A. Guenbour, I. Warad, and A. Zarrouk, *Synthesis, Surf. Interfaces* 18 (2020) 100442.
- [66] P. Singh, A. Singh, and M. Quraishi, *J. Taiwan. Inst. Chem. E* 60 (2016) 588.
- [67] G. Bahlakeh, A. Dehghani, B. Ramezanzadeh, and M. Ramezanzadeh, *J. Mol. Liq.* 293 (2019) 111559.
- [68] M. El Faydy, F. Benhiba, B. Lakhrissi, M. Ebn Touhami, I. Warad, F. Bentiss, and A. Zarrouk, *J. Mol. Liq.* 295 (2019) 111629.
- [69] M. El Faydy, H. About, F. Benhiba, B. Lakhrissi, A. Guenbour, F. Bentiss, I. Warad, E.E. Ebenso, and A. Zarrouk, *Surf. Interfaces* 20 (2020)100575.
- [70] T. Laabaissi, F. Benhiba, Z. Rouifi, M. Rbaa, H. Oudda, H. Zarrok, B. Lakhrissi, A. Guenbour, I. Warad, and A. Zarrouk, *Prot. Met. Phys. Chem. Surf.* 5 (2019) 1.